Ocean Engineering 153 (2018) 225–241

Contents lists available at ScienceDirect

Ocean Engineering

journal homepage: www.elsevier.com/locate/oceaneng

Numerical estimation of extreme waves and surges over the northwest Pacific Ocean

Jiangxia Li [a,b,c], Shunqi Pan [c], Yongping Chen [a,b,*], Yang-Ming Fan [d], Yi Pan [a,b]

[a] State Key Laboratory of Hydrology-Water Resources and Hydraulic Engineering, Hohai University, Nanjing 210098, China
[b] College of Harbor, Coastal and Offshore Engineering, Hohai University, Nanjing 210098, China
[c] Hydro-environmental Research Centre, School of Engineering, Cardiff University, Cardiff, CF24 3AA, United Kingdom
[d] Coastal Ocean Monitoring Center, National Cheng Kung University, Tainan 701, China

ARTICLE INFO

Keywords:
FVCOM circulation model
FVCOM-SWAVE wave model
ECMWF reanalysis wind data
Parametric typhoon model
Extreme waves and surges

ABSTRACT

A coupled modelling framework, consisting of the FVCOM circulation model and FVCOM-SWAVE wave model, was used to numerically estimate extreme waves and surges over the northwest Pacific Ocean. The ECMWF ERA-Interim atmospheric reanalysis data with modification by a parametric typhoon model were used as surface forcing to simulate waves and surges for a 35-year period. The extreme waves and surges with a 100-year return period were then estimated with the Gumbel distribution. The results showed that the extreme wave heights generally decreased northward and shoreward, varying from 23 m in deepwater areas to less than 7 m in nearshore areas. The extreme wave heights in the east and southeast directions were found to be larger than those in other directions; and the extreme waves in summer and autumn were found to be larger than those in other seasons. The extreme surge levels were relatively large in the radial sandy ridge area of the Jiangsu coast, Hangzhou Bay and north of the Qiongzhou Strait. This study demonstrated an effective approach to improve the representation of typhoon in the numerical estimation of extreme events. The results provide insights into the temporal and spatial distributions of extreme waves and surges over the northwest Pacific Ocean.

1. Introduction

The northwest Pacific Ocean region (Fig. 1) is the path of a large number of typhoons every year. The typhoons often come with strong winds and low sea surface pressures that generate extraordinarily large waves and surges and cause great damage to the affected areas. On the other hand, the rapid economic development and population growth have put this region under increasing pressure for a better protection from and reduced vulnerability to the extreme waves and high sea levels during typhoon events (Yin et al., 2011; Zhang and Sheng, 2015). To minimize and mitigate the damages caused by the extreme typhoons and to ensure a safe and effective design for ocean and coastal engineering projects, it is desirable and essential to gain a better understanding of the temporal and spatial distributions of the extreme waves and surges in both offshore and nearshore areas.

In recent years, there have been a number of studies focused on the spatial and temporal distribution features of mean and extreme waves in this region based on the analysis of field observational data or remote sensing data (Yao et al., 1992; Qi et al., 1997; Wang and Yi, 1997; Liu and Sun, 2000; Chen et al., 2006a,b). There have also been studies on the spatial and temporal distribution of extreme sea levels based on the analysis of tide gauge observation data (Xu and Huang, 2011; Li and Li, 2013; Feng and Tsimplis, 2014; Feng and Jiang, 2015). However, because of the limited observation data, the results from those studies are only applicable to local areas, which may not be adequate for large domains such as the northwest Pacific Ocean region.

With significant advancement in computing techniques and power, numerical modelling has become an effective way to study the long-term wave climate over the northwest Pacific Ocean region. Third-generation spectral wave models such as WAM (WAMDIG, 1988), WAVEWATCH III (Tolman, 1991) or SWAN (Booij et al., 1999) are commonly used for wave modelling. A series of wind data, which usually comes from a global or regional reanalysis dataset, is used to drive the wave model for long-term wave hindcasting and analysis of the wave characteristics in an entire study region. For example, Lv et al. (2014) used the ECMWF (European Centre for Medium-Range Weather Forecasts) reanalysis wind data to drive the SWAN model to perform a 20-year wave hindcasting in the Bohai Sea; then, the annual and seasonal distributions of mean wave

* Corresponding author. State Key Laboratory of Hydrology-Water Resources and Hydraulic Engineering, Hohai University, Nanjing 210098, China.
E-mail address: ypchen@hhu.edu.cn (Y. Chen).

https://doi.org/10.1016/j.oceaneng.2018.01.076
Received 19 January 2017; Received in revised form 27 April 2017; Accepted 16 January 2018

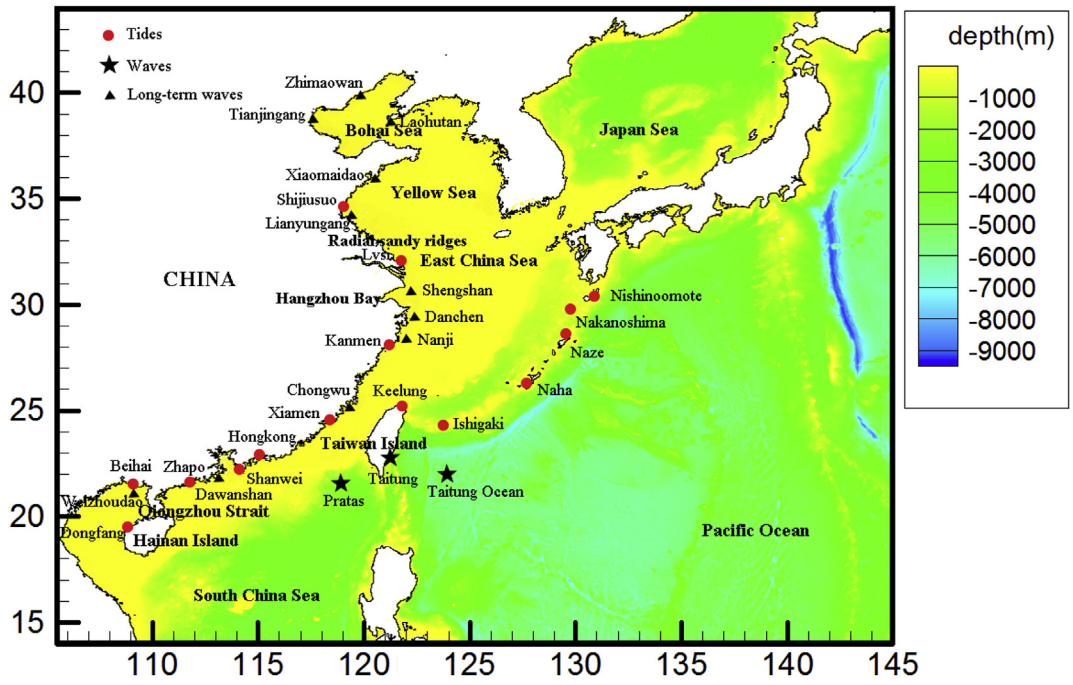

Fig. 1. The northwest Pacific Ocean region and locations of tide and wave observation stations.

characteristics in the Bohai Sea were analysed. Liang et al. (2014) used the wind data obtained from the Weather Research and Forecasting (WRF) Model to drive the SWAN model for a 22-year wave hindcasting in the Bohai Sea, Yellow Sea and East China Sea (BYECS); the spatial distributions of mean and largest significant wave heights in four seasons in BYECS were then specified. Zheng and Li (2015) used the CCMP (Cross-Calibrated Multi-Platform) surface wind data to drive the WAVEWATCH III model for a 24-year wave hindcasting, and the annual distributions of mean wave height and wave power density in the China Sea were discussed in detail.

In addition to the analysis of mean wave characteristics, numerical modelling has also been applied to estimate the extreme waves over a large domain. Lee and Jun (2006) used the ECMWF reanalysis wind data to drive the WAM model for a 25-year wave hindcasting, and simulated the typhoon waves for 106 major typhoons that affected the waters around the Korean Peninsula individually. The design wave heights for the return periods of 10, 20, 30, 50 and 100 years for 16 directions were estimated by means of the extreme wave analysis method. Chen et al. (2013) used the NCEP/NCAR (National Centers for Environmental Prediction/National Centre for Atmospheric Research) reanalysis wind data to drive the WAM wave model for hind-casting waves over 60 years in the East China Seas, and the results were used to estimate the extreme waves with 50-year and 100-year return periods. Li et al. (2016a) used both NCEP and ECMWF wind data to drive the WAM wave model and calculated the extreme waves in the same region. Waves with a 100-year return period generated by both wind datasets were compared with those measured at several observation stations along the China coasts. Although the ECMWF wind data were regarded relatively better in terms of resolution than other wind datasets (e.g. NCEP/NCAR), the extreme waves were found in general underestimated in comparison with the measurements, indicating the necessity for improvement of the original ECMWF wind data, particularly during the period of typhoon events. Li et al. (2016b) applied the method proposed by Pan et al. (2016) of modifying the ECMWF reanalysis data and found that the modified wind field considerably improved the accuracy of simulated extreme waves in the China Seas. Although a number of relevant studies have shown the feasibility of using wave models to reveal the temporal and spatial distributions of extreme waves over the entire region of the northwest Pacific Ocean, further detailed research is still much needed to obtain a more accurate estimation.

Apart from the extreme waves, the determination of extreme surges is also important for the design of coastal and offshore structures. Considering its destructive power, the relevant literature on modelling of storm surge has usually focussed on the temporal and spatial distribution of storm surge during a single storm event (Guo et al., 2009; Zhang et al., 2007; Beardsley et al., 2013; Yoon et al., 2014). Recently, Zhang and Sheng (2015) used the NCEP/CFSR (Climate Forecast System Reanalysis) wind data to drive the POM (Princeton Ocean Model) for a period of 32 years and analysed the extreme sea levels from surges and tides in the northwest Pacific Ocean. However, studies using coupled wave-current models for detailed analyses of spatial and temporal variations of extreme surges, especially from long-term simulations, are still lacking. Given the strong nonlinear interaction between waves and currents during typhoon periods, especially in the coastal area (Yoon and Jun, 2015), it is essential to consider the effects of wave-current interaction in long-term simulations to study the extreme waves and surges.

In this study, a coupled modelling framework, which consisted of the FVCOM circulation model and FVCOM-SWAVE, was set up over the northwest Pacific Ocean region for hindcasting waves and surges for a period of 35 years from 1979 to 2013. The modelling system was driven by the surface forcing based on the newly released ECMWF ERA-interim reanalysis data, and the tide forcing at the open boundaries from TPXO 7.2 data (Egbert and Erofeeva, 2002). To take account for the effects on typhoons events occurred in the region, the ECMWF data were also modified by a parametric typhoon model as proposed by Pan et al. (2016). The hindcasting results were then used to estimate the temporal and spatial distributions of extreme waves and surges over the entire northwest Pacific Ocean region.

The paper is organized as follows. The description of the wave and surge model used for the hindcasting and the method used for extreme analysis of annual maxima is presented in Section 2. The details of model setup and model validation are presented in Sections 3 and 4, respectively. The results of mean and extreme waves with a 100-year return period are presented and discussed in Section 5. The results of extreme surges with a 100-year return period are presented in Section 6, followed by a few conclusions in Section 7.

2. Methodology

2.1. Modelling framework

The modelling framework used in this study was the coupled 3D circulation model FVCOM and the wave model FVCOM-SWAVE. Whilst the details of each model can be found elsewhere (Chen et al., 2006a,b; Qi et al., 2009), both models and the principal governing equations used are briefly described here.

2.1.1. FVCOM model

The FVCOM model is a prognostic, unstructured-grid, Finite-Volume, free-surface, three-dimensional (3-D) primitive equations Community Ocean Model developed originally by Chen et al. (2003). By using an unstructured triangular mesh, the model is capable of resolving complex geometry and bathymetry. With Boussinesq and hydrostatic approximations, the governing equations (momentum and continuity) in σ-coordinates are as follows:

$$\frac{\partial(Du)}{\partial t}+\frac{\partial(Du^2)}{\partial x}+\frac{\partial(Duv)}{\partial y}+\frac{\partial(u\omega)}{\partial\sigma}-fvD = -\mathrm{gD}\frac{\partial(\eta-\eta_a)}{\partial x}-\frac{\mathrm{g}D^2}{\rho_0}\int_\sigma^0\left[\frac{\partial\rho}{\partial x}-\frac{\sigma}{D}\frac{\partial D}{\partial x}\frac{\partial\rho}{\partial\sigma}\right]d\sigma+\frac{\partial}{\partial\sigma}\left[\frac{K_m}{D}\frac{\partial u}{\partial\sigma}\right]+F_u \quad (1)$$

$$\frac{\partial(Dv)}{\partial t}+\frac{\partial(Duv)}{\partial x}+\frac{\partial(Dv^2)}{\partial y}+\frac{\partial(v\omega)}{\partial\sigma}+fuD = -\mathrm{gD}\frac{\partial(\eta-\eta_a)}{\partial y}-\frac{\mathrm{g}D^2}{\rho_0}\int_\sigma^0\left[\frac{\partial\rho}{\partial y}-\frac{\sigma}{D}\frac{\partial D}{\partial y}\frac{\partial\rho}{\partial\sigma}\right]d\sigma+\frac{\partial}{\partial\sigma}\left[\frac{K_m}{D}\frac{\partial v}{\partial\sigma}\right]+F_v \quad (2)$$

$$\frac{\partial\eta}{\partial t}+\frac{\partial(Du)}{\partial x}+\frac{\partial(Dv)}{\partial y}+\frac{\partial\omega}{\partial\sigma}=0 \quad (3)$$

where x, y, and σ are the east, north, and vertical directions in the Cartesian coordinate system; u, v, and ω are the velocity components in x, y and z, respectively; f is the Coriolis coefficient; g is the gravitational acceleration; $\mathrm{K_m}$ is the vertical eddy viscosity coefficient; ρ_0 is the reference density; ρ is the perturbation density; $D=H+\eta$ is the total water depth where H is the reference depth below the mean sea level and η is the surface elevation. η_a is the sea level displacement induced by the atmospheric pressure perturbation's inverted barometer effect; and $\mathrm{F_u}$ and $\mathrm{F_v}$ are the horizontal momentum diffusion terms. The baroclinic dynamics is excluded in this study.

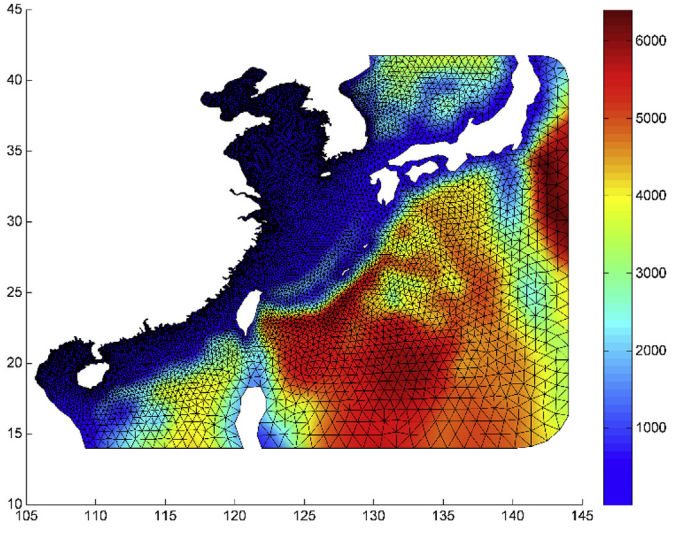

Fig. 2. The model mesh and bathymetry (m).

2.1.2. FVCOM-SWAVE model

The FVCOM-SWAVE model is an unstructured grid version of the surface wave model developed by Qi et al. (2009), who implemented the finite-volume algorithms within the SWAN model (Booij et al., 1999). This model provides an alternative option for unstructured-grid wave models for the coastal ocean. The FVCOM-SWAVE model can also be coupled with any triangular mesh-based unstructured-grid ocean models for the study of current-wave interactions. The main governing equation is the spectral action balance equation.

$$\frac{\partial N}{\partial t}+\nabla\cdot\left[(\vec{C}_g+\vec{V})N\right]+\frac{\partial C_\sigma N}{\partial\sigma}+\frac{\partial C_\theta N}{\partial\theta}=\frac{S_{tot}}{\sigma} \quad (4)$$

where N is the wave action density spectrum, t is the time, σ is the relative frequency, θ is the wave direction, C_σ and C_θ are the wave propagation velocities in spectral space (σ, θ), $\vec{C}_g$ is the group velocity, and $\vec{V}$ is ambient water current vector. S_{tot} is the source-sink term defined as:

$$S_{tot}=S_{in}+S_{nl3}+S_{nl4}+S_{ds,w}+S_{ds,b}+S_{ds,br} \quad (5)$$

where S_{in} is the function for wind-induced wave growth, S_{nl3} is the nonlinear transfer of wave energy from three-wave interactions, S_{nl4} is the nonlinear transfer of wave energy from four-wave interactions, $S_{ds,w}$ is the wave decay from white capping, $S_{ds,b}$ is the wave decay from bottom friction, and $S_{ds,br}$ is the wave decay from depth-induced wave breaking.

2.1.3. Coupled FVCOM and FVCOM-SWAVE models

As described in Wu et al. (2011), the coupled FVCOM and FVCOM-SWAVE models have been used to study nearshore and ocean hydrodynamic processes such as tides, circulations, storm surge and waves. The coupling between the FVCOM model and the FVCOM-SWAVE model is achieved by incorporating 3D radiation stress, wave-current-related bottom boundary layer and sea surface stress parameterizations. After the initialization, the wave model calculates significant wave height, wave direction, average wave length, surface wave relative peak period, wave bottom orbit velocity, and bottom wave period. The radiation stresses or surface stresses are passed to the circulation model after the completion of the wave computation. The results of current and water surface elevation from the circulation model are fed back to the wave model for the wave-current interaction to be considered for simulations at the next time step.

2.2. Long-term wave statistics analysis method (Gumbel distribution)

In general, the extreme waves and surges with a given return period can be estimated using a particular statistical method. The Gumbel distribution is one of the most commonly used methods to estimate the extreme values in the design of coastal engineering, also known as the extreme value type I distribution (Hong et al., 2013). The Gumbel distribution is given by Castillo (1988) as:

$$\mathrm{F(x)}=\exp\{-\exp[-\alpha(\mathrm{x}-\mathrm{u})]\} \quad (6)$$

where F(x) denotes the cumulative distribution function; x denotes the value of the random variable X; and u and α are the location and scale parameters, respectively. Relation $\mathrm{Y}=\alpha(\mathrm{X}-\mathrm{u})$ represents the standardized or reduced extreme variety. The mean of X, μ_x and its standard deviation, σ_x, are given in Equations (7) and (8),

$$\mu_x=u+\frac{\gamma}{\alpha} \quad (7)$$

$$\sigma_x=\frac{\pi}{\sqrt{6}\alpha} \quad (8)$$

Table 1
Details of numerical experiments.

Case	Tide	Wind & Air Pressure	Output
CASE-TO	Yes	No	Tide
CASE-WC1	Yes	ECMWF	Tide & Wave
CASE-WC2	Yes	ECMWF-T	Tide & Wave

a. Tidal level validation.

where $\gamma \approx 0.5772$ is a Euler constant.

For a given T-year return period, the value of X, x_T, can be estimated by using the following equation,

$$x_T = u - \frac{1}{\alpha}\ln\left[-\ln\left(1-\frac{1}{T}\right)\right] \quad (9)$$

3. Model setup

3.1. Computational domain

In this study, the computational domain for the coupled model covers the northwest Pacific Ocean region, which includes the Bohai Sea, the Yellow Sea, the East China Sea, the northern part of the South China Sea and the southern part of the Japan Sea, as shown in Fig. 1. The model used an unstructured mesh with a resolution of 1° at the open boundaries and finer than 0.1° in the coastal areas. There were 12 077 nodes and 22 562 elements in this mesh. The bathymetric data were obtained from the General Bathymetric Chart of the Oceans (GEBCO) 30 arc-second global bathymetric dataset (http://www.gebco.net/data_and_products/gridded_bathymetrydata/) with corrections at the nearshore areas using available ocean maps and then interpolated onto the model grid. The model mesh and bathymetry are shown in Fig. 2.

3.2. Model forcing

Along the open boundaries of the computational domain, tidal forcing was used to drive the model with tidal levels imposed on the north, east and south open boundaries. The tidal levels along the open boundaries were calculated with 13 tidal constituents (M2, S2, N2, K2, K1, O1, P1, Q1, Mf, Mm, M4, MS2 and MN4) from the global tidal model TPXO 7.2. All the constituents are corrected by the 18.6-year nodal cycle in this study by considering the contribution of nodal modulation to tidal amplitudes (Haigh et al., 2011).

For the surface forcing, the model was driven by 6-hourly atmospheric pressure at the sea surface level and the wind velocity at 10 m above the sea surface, based on the ECMWF ERA-Interim global atmospheric reanalysis data that modified by a parametric typhoon model, as described below. The resolution of the ECMWF data field is T255 (triangular truncation at 255), N128 (128 latitude circles, pole to equator), which corresponds to approximately 79 km on the reduced Gaussian grid while the data used in this study was the version interpolated to 0.125° grid. The data was regarded finer than many other reanalysis data

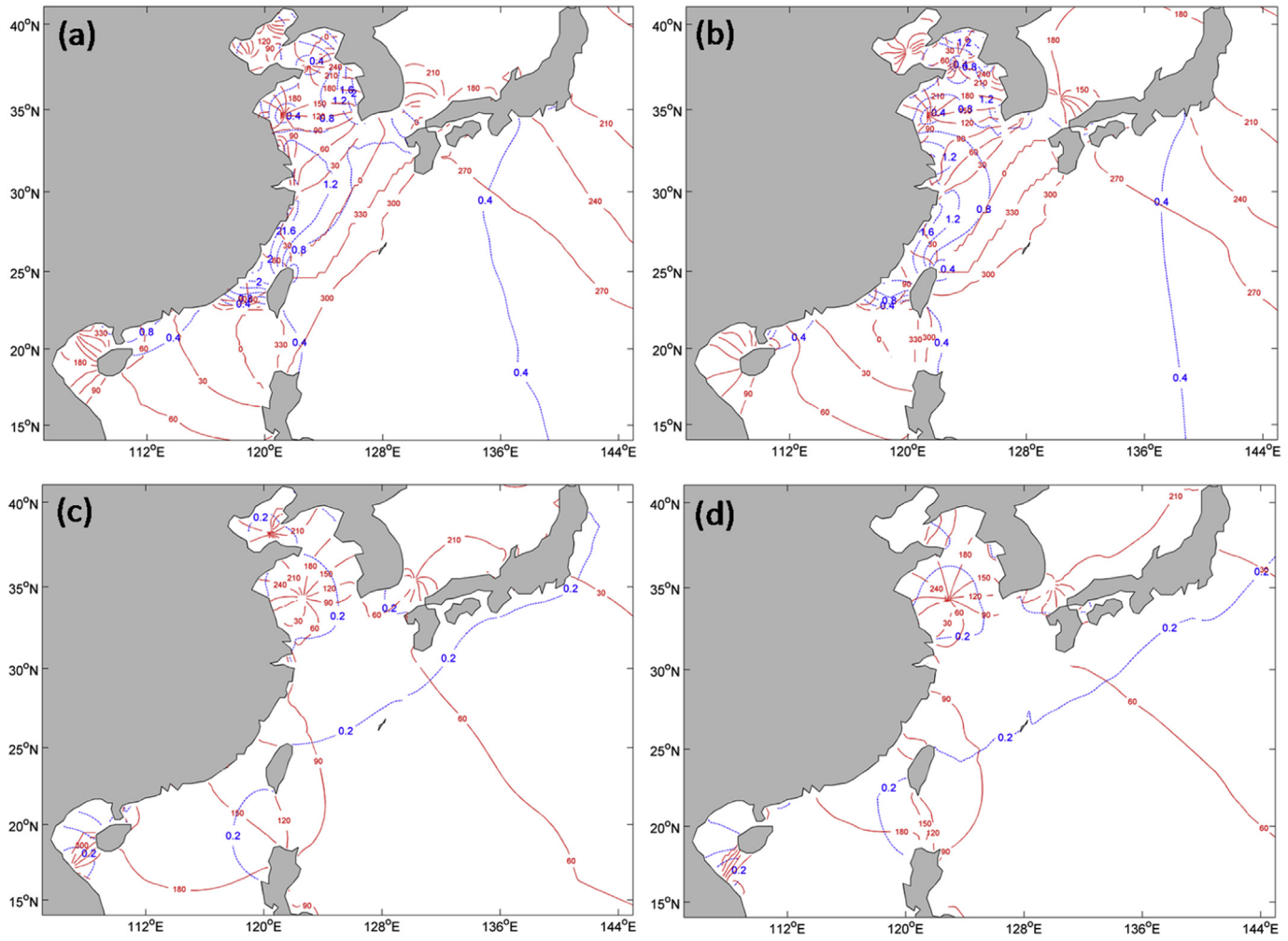

Fig. 3. Comparisons of co-amplitudes (blue dash line) and co-phases (red solid line, Greenwich phase) of tidal constituents M_2 (a - Model & b - TPXO) and K_1 (c – Model & d – TPXO) in year 1995. (For interpretation of the references to colour in this figure legend, the reader is referred to the Web version of this article.)

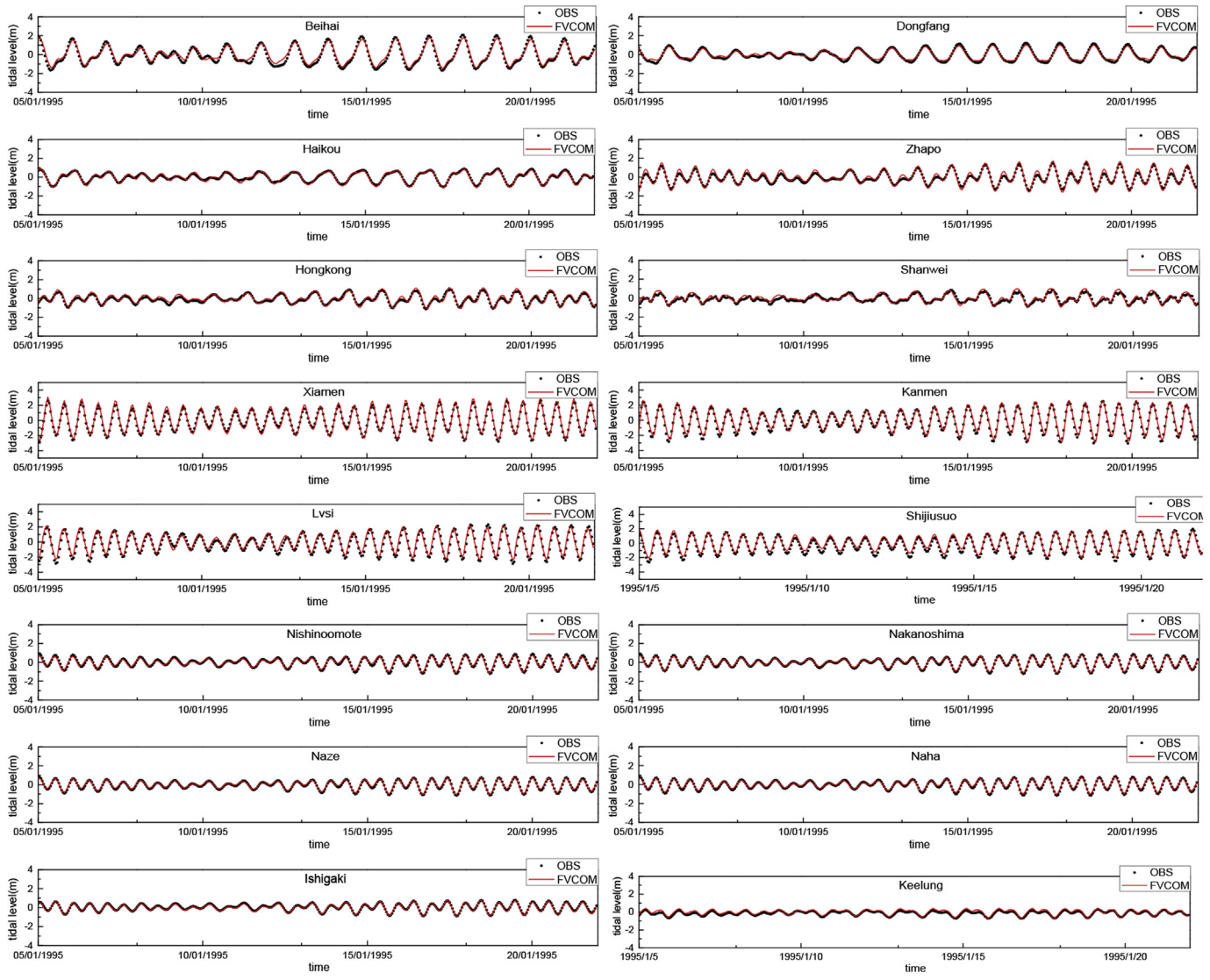

Fig. 4. Comparison of tidal levels between measured and simulated data at 16 gauge stations.

sets available such as that from NCEP (Kalnay et al., 1996; Li et al., 2016a).

3.3. Parametric typhoon model

The existing resolution of reanalysis wind data provided by ECMWF, as suggested by earlier studies (Jourdain et al., 2014; Li et al., 2016b), is insufficient to represent the atmospheric forcing of typhoon events; therefore, a parametric typhoon model as introduced by Jelesnianski (1965) was used to generate typhoon wind field and air pressure near the typhoon centre for a better representation of the typhoon's effects. The parametric typhoon model was based on the measured typhoon tracks from the "best track dataset" provided by China Meteorological Administration Tropical Cyclone Data Centre (http://tcdata.typhoon.gov.cn/). The concept and formulations used in the parametric typhoon model are described as follows.

$$p(r) = \begin{cases} \frac{\rho_a}{3}\left(\frac{V_R}{\gamma}\right)^2\left(\frac{r}{R}\right)^3 + p_0 & 0 \le r \le R \\ -\rho_a\left(\frac{V_R}{\gamma}\right)^2\frac{R}{r} + p_\infty & r > R \end{cases} \tag{10}$$

$$V(r) = \begin{cases} V_R\left(\frac{r}{R}\right)^{3/2} + V_{SR}\frac{r}{R+r} & 0 \le r \le R \\ V_R\left(\frac{R}{r}\right)^{1/2} + V_{SR}\frac{R}{R+r} & r > R \end{cases} \tag{11}$$

where $p(r)$ is the sea surface pressure; $V(r)$ is the wind speed at radius r with respect to the typhoon centre; ρ_a is the air density, p_0 is the air pressure at the centre and p_∞ is the air pressure at great distance from the centre; V_R is the maximum wind speed at distance R from its centre, and V_{SR} is the moving velocity of the typhoon centre. R is the radius at which the maximum wind speed occurs and is calculated according to the method suggested by Knaff et al. (2007). The value of γ can be calculated by:

$$\gamma = 2V_R\sqrt{\frac{\rho_a}{3(p_\infty - p_0)}} \tag{12}$$

As the typhoon centre in the reanalysis data might not always coincide with the one in the parametric typhoon model (Jourdain et al., 2014), a shift of the reanalysis wind and pressure field was made before blending the typhoon model wind and pressure field into the original reanalysis data (Pan et al., 2016), and then a smoothening technique was used to ensure that the wind field was generally continuous,

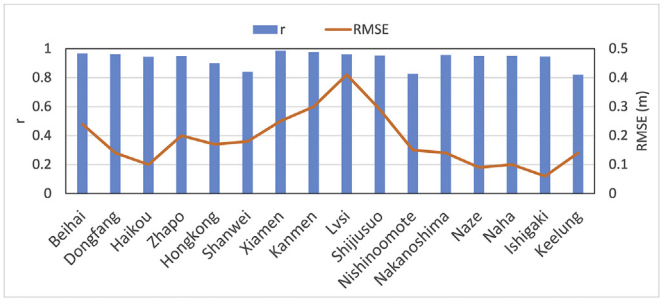

Fig. 5. Correlation Coefficient (r) and root mean square error (RMSE) between the measured and simulated tidal levels at 16 observation stations.

$$V = (1 - e)V_{ECMWF} + eV_{TY} \tag{13}$$

where V is the modified wind speed, V_{ECMWF} is the original reanalysis ECMWF wind speed, V_{TY} is the wind speed of the parametric typhoon wind field, and e is the weight coefficient, which can be calculated by,

$$e = \frac{r - R_1}{R_2 - R_1} \tag{14}$$

where R_1 and R_2 are the two boundary limits of the transition region of the blended data. Eq. (13) is also applicable to sea surface air pressure.

4. Model validation

The numerical model was first validated with the field measurements for tides and waves. The locations of the measurements for tides and waves are shown in Fig. 1. Because of the availability of the field data, the model validations were carried out for tides and surge levels in 1995 and for waves between June and Oct 2012. The majority of the water level measurements were taken along the coastal areas of China, and wave data measurements were taken in the offshore area of the southern Taiwan Island. Three numerical experiments were considered: CASE-TO is the tide only case, and CASE-WC1 and CASE-WC2 are for the combined tide and wave conditions. CASE-WC1 was driven by original or unmodified ECMWF reanalysis wind and surface atmospheric pressure (denoted as ECMWF) and the CASE-WC2 was driven by the wind and surface atmospheric pressure integrated with the results of the parametric typhoon model for a better presentations of typhoon effects (denoted as ECMWF-T), as listed in Table 1.

For tidal level validation, the model was run in the tide-only mode (CASE-TO) over the entire year of 1995 because of the availability of field data. The amplitudes and phased of principle tidal constituents M_2 and K_1 are calculated from the CASE-TO results and compared with that from the TPXO dataset as shown in Fig. 3. It can be seen that the amplitudes and phases of the M_2 and K_1 tides produced by the FVCOM model are in good agreement with those generated by the TPXO 7.2 database, especially for the area near China coasts. The simulated amplitudes and phases are also found to be comparable with the previous numerical or observational studies within the northwest Pacific Ocean of Fang et al. (2004), Song et al. (2013) and Zhang and Sheng (2015).

To validate the model on tide levels, the measurements taken from 16 tide gauge stations in the northwest Pacific Ocean region (see Fig. 1), provided by the Sea Level Centre at the University of Hawaii (UHSLC: http://uhslc.soest.hawaii.edu; Caldwell et al., 2015) are used. Fig. 4

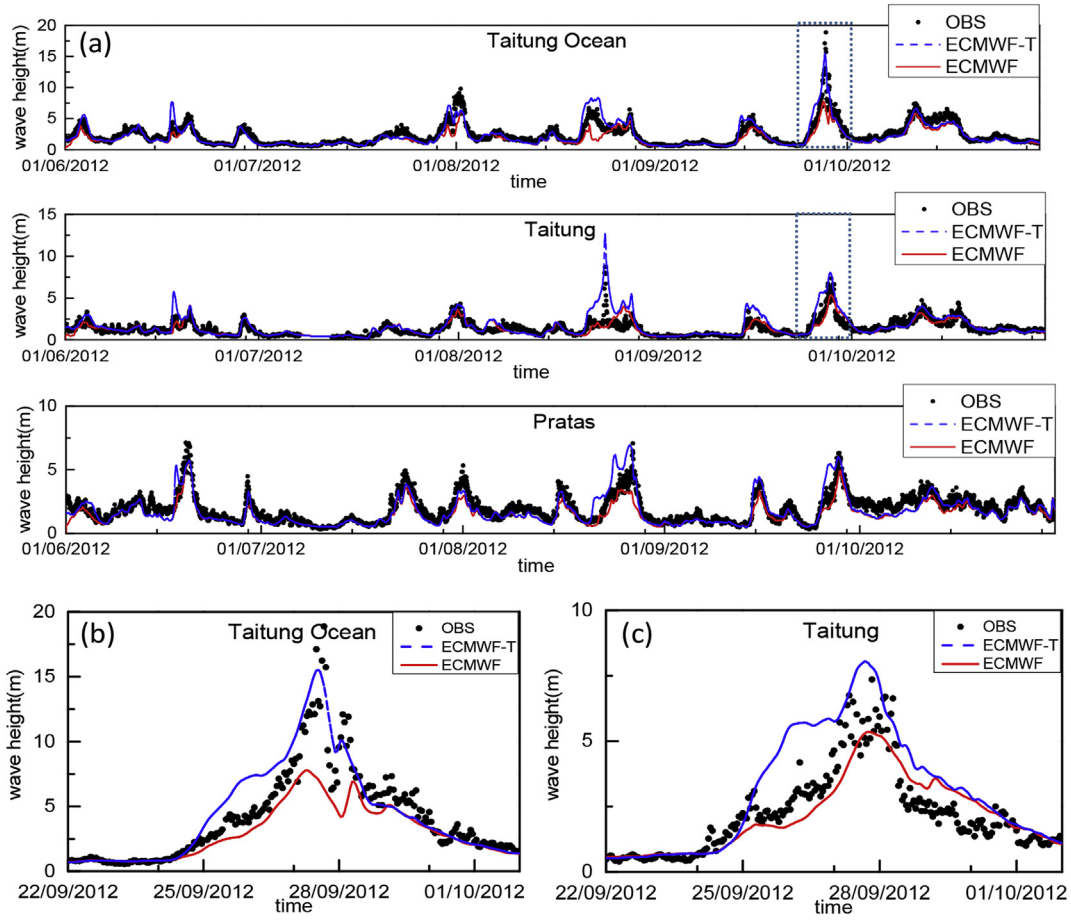

Fig. 6. (a) Comparison of measured (Obs) and simulated wave heights at Taitung Ocean, Taitung and Pratas Stations; (b) and (c) detailed comparisons at the typhoon peak on 27/09/2012 at Taitung Ocean and Taitung Stations.

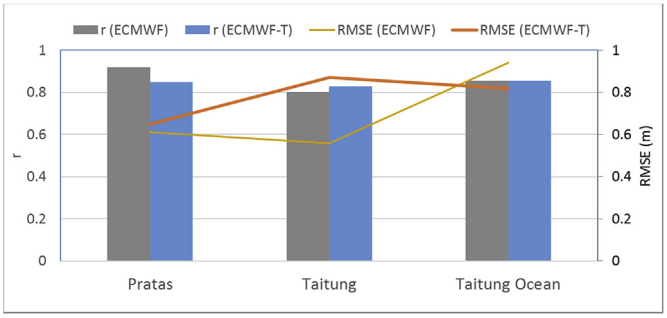

Fig. 7. Correlation coefficient (r) and root mean square error (RMSE) between measured and simulated wave heights (forced by ECMWF and ECMWF-T data) at 3 observation stations.

shows the comparisons of tidal levels between simulations and observations at 16 gauge stations from the 5th to the 21st of January 1995 over a spring-neap tide cycle. It can be seen from Fig. 4 that the simulated tidal level generally agreed well with the observational data for both tidal range and tidal phase.

To further quantify the model performance in predicting tidal levels, the correlation coefficients (r) and root mean square errors (RMSE) between the computed and measured tidal levels (defined below) were calculated by the following equations:

$$r = \frac{\sum_{i=1}^{n}(x_i - \bar{x})(y_i - \bar{y})}{\sqrt{\sum_{i=1}^{n}(x_i - \bar{x})^2}\sqrt{\sum_{i=1}^{n}(y_i - \bar{y})^2}} \quad (15)$$

$$RMSE = \sqrt{\frac{1}{n}\sum_{i=1}^{n}(x_i - y_i)^2} \quad (16)$$

The correlation coefficient (r) indicates the fit level between the observed and simulated quantities and RMSE measures their deviations. Fig. 5 shows the correlation coefficients and RMSEs of the validation results at 16 stations. It is clear that all correlation coefficients were over 0.8 and the RMSEs were no more than 0.3 m except at Lvsi because of a very complicated bathymetry near the radial sandy ridge area in the Southern Yellow Sea (Xu et al., 2016). In general, as seen from the results shown in both Figs. 4 and 5, the simulated tidal levels agreed well with the observational data, which indicates that the modelling system performed well in simulating the tidal levels in the study area.

4.1. Wave validation

With the combined tide and wave conditions, the computed significant wave heights generated by the un-modified ECMWF reanalysis wind data (CASE-WC1) and the modified ECMWF-T wind data (CASE-WC2) were compared with the measurements from three wave buoys (Taitung Ocean Station with depth of approximately 5 600 m; Taitung Station and Pratas Station with depth of approximately 2 600 m) in the southern coastal water of Taiwan (see Fig. 1). Fig. 6 (a) shows the comparison of measured and the simulated wave heights between June and October 2012. It can be seen from Fig. 6 (a) that the waves generated by both wind fields generally agreed with the observational data. However, in the simulation of large waves during the typhoon periods, for example, those in 27 September 2012 as shown in Fig. 6 (b) and (c), the waves generated in CASE-WC2 agreed better. Fig. 7 shows the values of correlation coefficients and RMSEs between simulated and observed data. The RMSEs at all the three stations were less than 1 m, whereas the extreme wave heights at these stations were greater than 5 m and up to 10 m in some

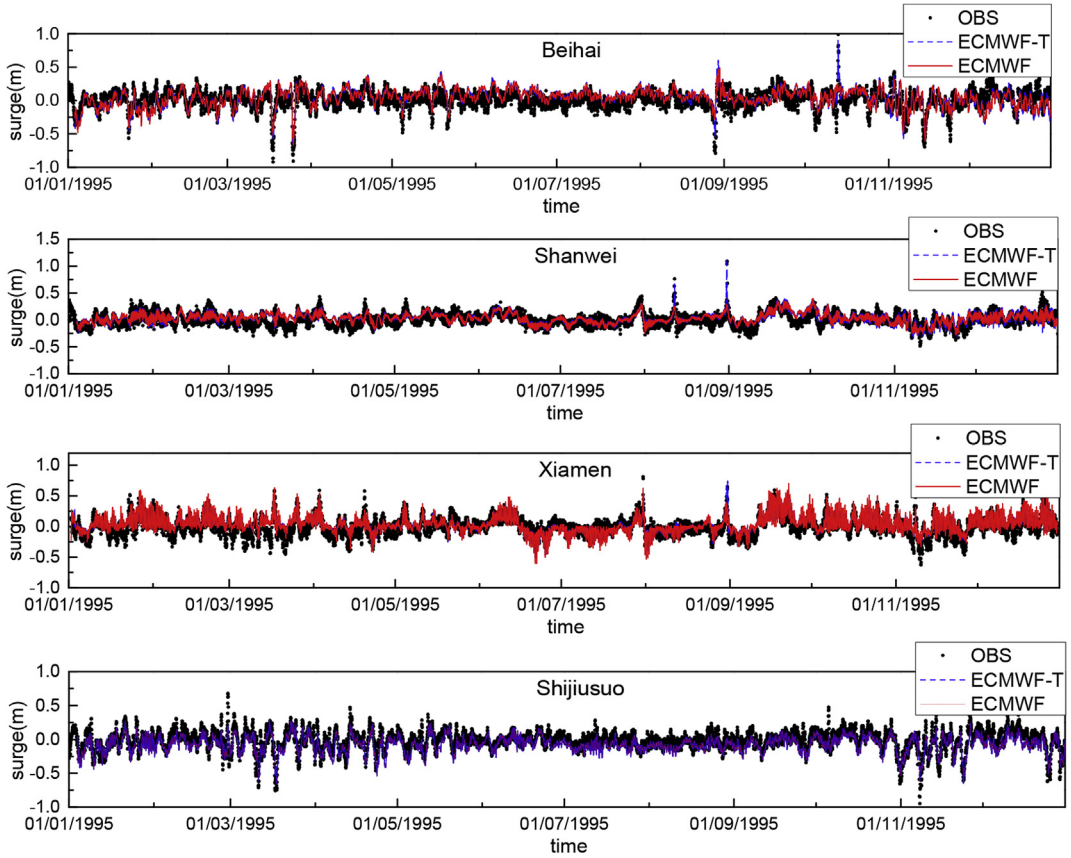

Fig. 8. Comparison of measured and simulated surge levels with ECMWF and ECMWF-T data at 4 selected tide gauge stations.

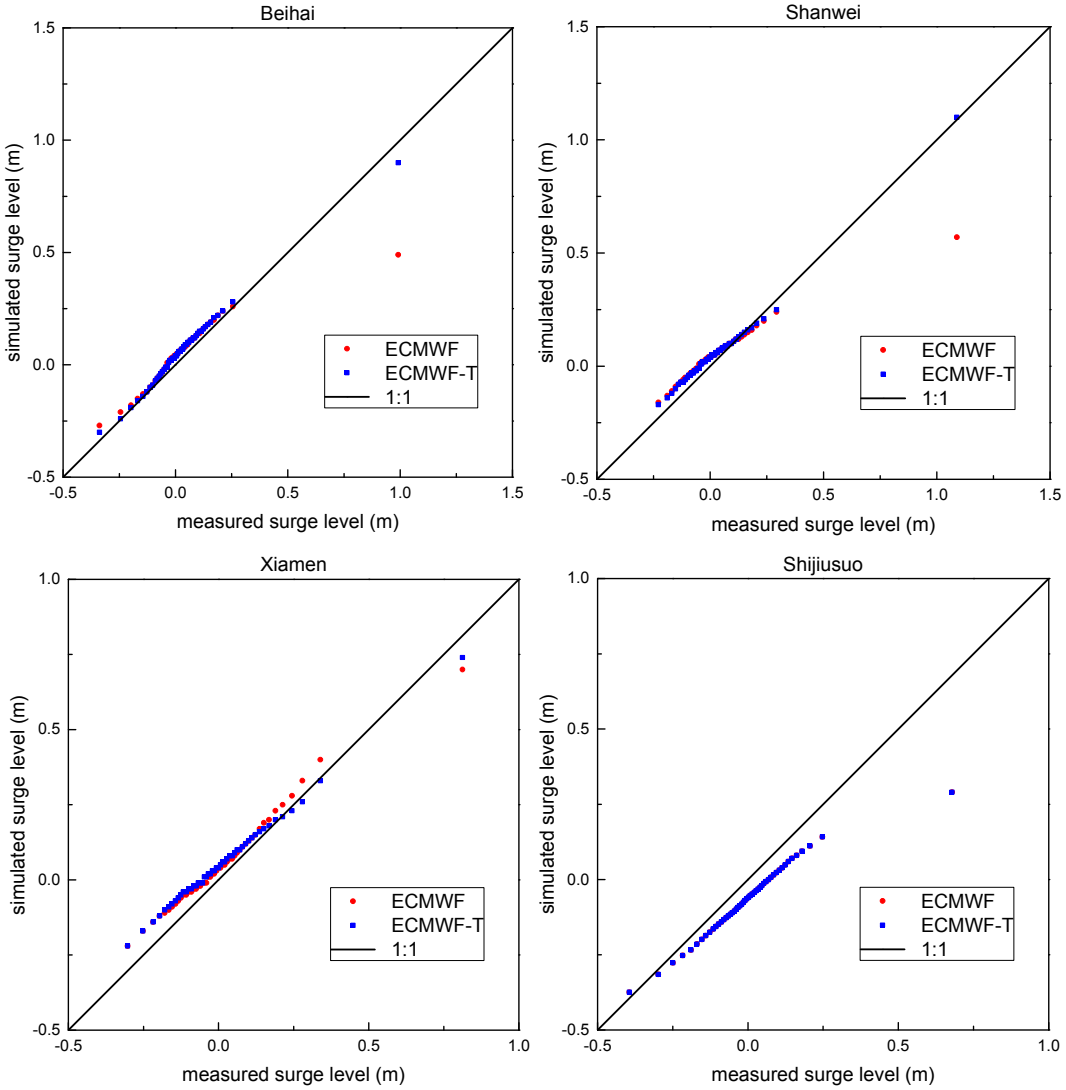

Fig. 9. Q-Q plots of the measured and simulated surge levels using ECMWF and ECMWF-T data at the Beihai, Shanwei, Xiamen and Shjiusuo tide gauge stations.

cases, which can be regarded as satisfactory. The values of correlation coefficients for waves generated by ECMWF-T showed better correlations at Taitung Station compared with the results for the un-modified ECMWF data. However, at Pratas Station, the correlation was slightly less satisfactory. Wave heights at this station were the lowest among all stations because the typhoon centres were far from the station. In this case, the modification of typhoon winds might be less effective; nonetheless, the mean wave heights were reasonably predicted compared with the field measurements. In general, the results demonstrated the improvement of the wave predictions gained from the modified ECMWF data (ECMWF-T).

4.2. Surge validation

For storm surge, the model was run with conditions for the entire year of 1995. The simulated storm surge was calculated by subtracting the water levels from the tide-only model (CASE-TO) from those from the model driven by wind and sea level pressure using ECMWF and ECMWF-T data (CASE-WC1 and CASE-WC2). The tidal and non-tidal components of the observation sea levels were extracted using a harmonic analysis package known as T_TIDE (Pawlowicz et al., 2002). Fig. 8 shows the comparison of the simulated surge levels from both ECMWF and ECMWF-T data with the observations at four selected tide gauge stations (Beihai, Shanwei, Xiamen and Shijiusuo) from the south to the north coast as shown in Fig. 1. It can be seen from Fig. 8 that the simulated surges from both wind data sets fit the observational data well.

For further comparison, the Quantile-Quantile (Q-Q) plots for the simulated and observed surge levels at the four observation stations are given in Fig. 9. It can be seen that the extremely large surges simulated by ECMWF-T generally agreed better with the observational data than those generated by ECMWF, especially at Beihai and Shanwei, because of the better performance of ECMWF-T data in the simulation of large storm surges during the typhoon periods, whereas the surges were underestimated when using the original ECMWF data. However, the improvement of ECMWF-T at Shijiusuo Station appears to have been minimal; the maximum surge levels were under-predicted using both ECMWF and ECMWF-T at almost an identical level because the extreme surges generated by the cold storms in winter seasons were more significant than those by typhoons at this station. However, it should be noted that the overall surge levels here were much lower than at other stations.

4.3. Wave-current effects during typhoon periods

According to Yoon and Jun (2015), the nonlinear interaction between waves and currents are strong during typhoon periods, especially in the

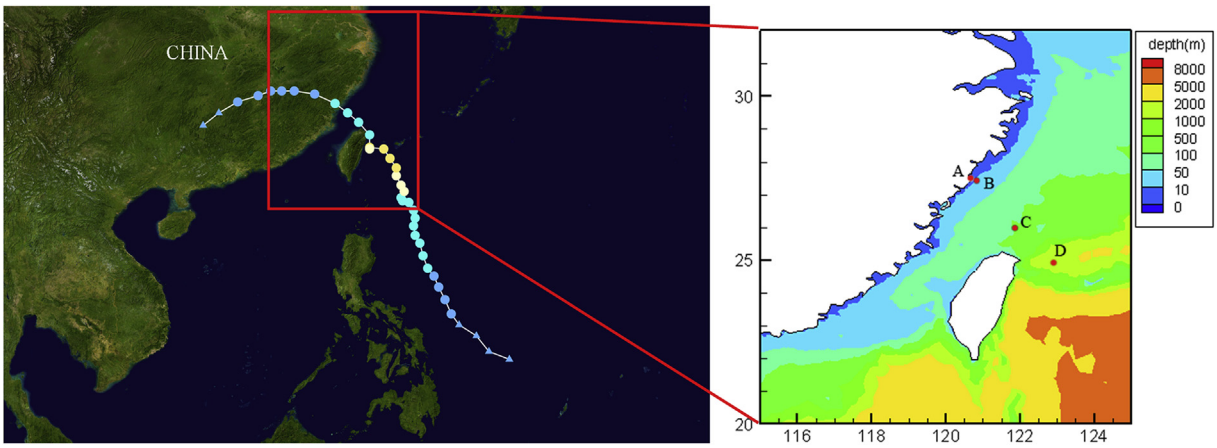

Fig. 10. Typhoon track of Saola and 4 locations.

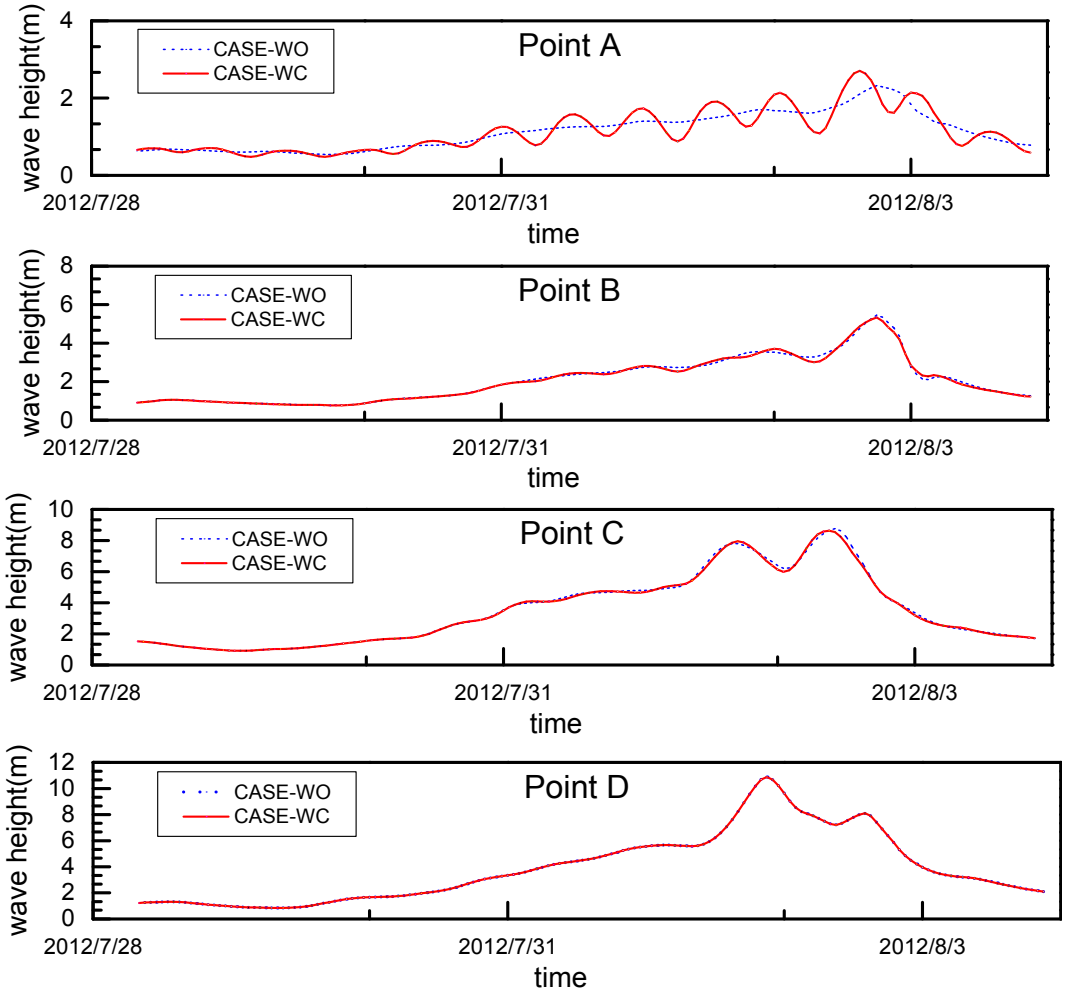

Fig. 11. Comparisons of the significant wave heights computed by coupled (CASE-WC) and uncoupled (CASE-WO) model during typhoon Saola at four examining locations.

coastal area. In order to understand the effects of wave-current interaction on wave and surge simulations under the extreme conditions, Typhoon Saola (the ninth named storm in 2012) was chosen as an example to illustrate the effect of the wave-current interaction using the coupled and uncoupled models at 4 examining locations in present study. Fig. 10 shows the track of Saola and four examining locations nearshore which are close to the typhoon centre. The water depths for locations A, B, C, and D are 7.9 m, 21.4 m, 115.9 m and 1 527.4 m respectively.

The effects of the wave-current interaction were examined by running both coupled and uncoupled models, i.e. CASE-WC and CASE-WO, and comparing the simulated wave height at four locations as shown in Fig. 11 during typhoon Saola. It can be seen that at the shallow water

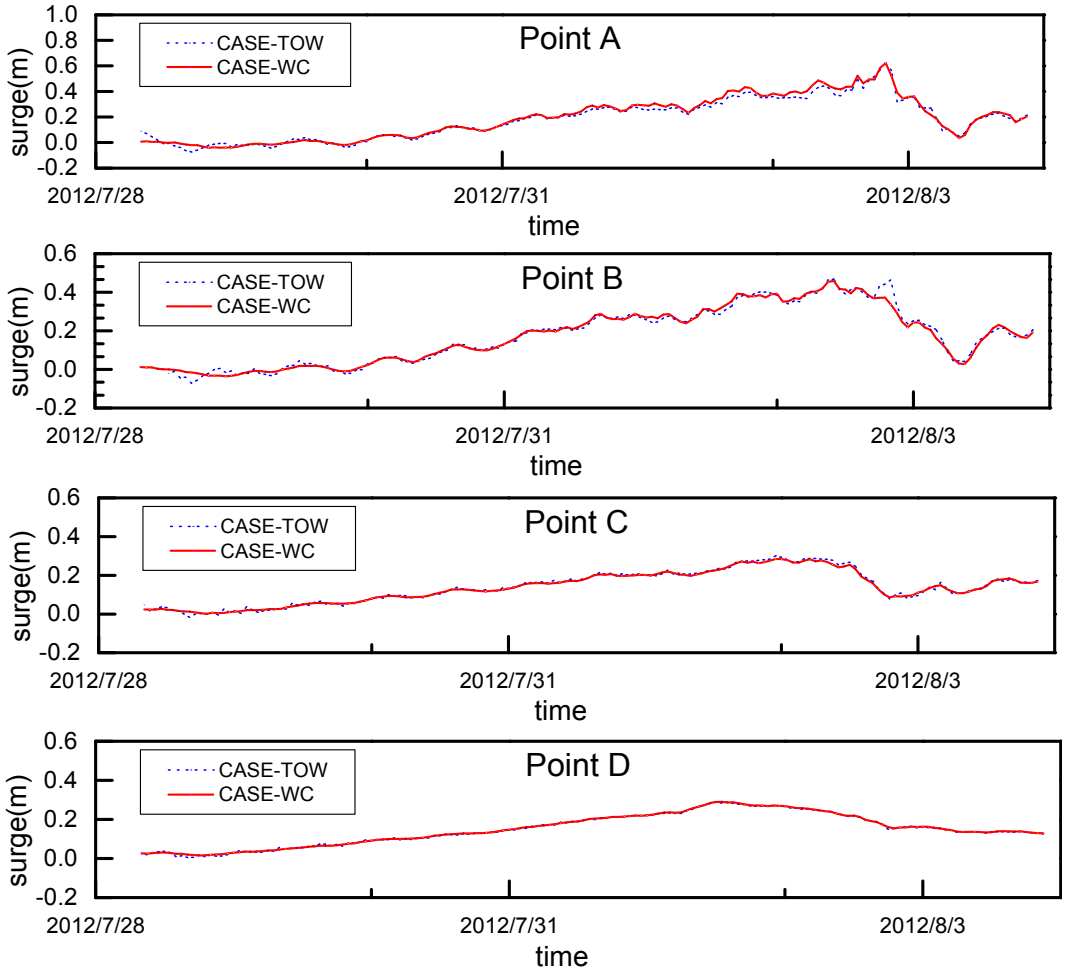

Fig. 12. The simulated surge between coupled (CASE-WC) and uncoupled (CASE-TOW) model during typhoon Saola at four representative points.

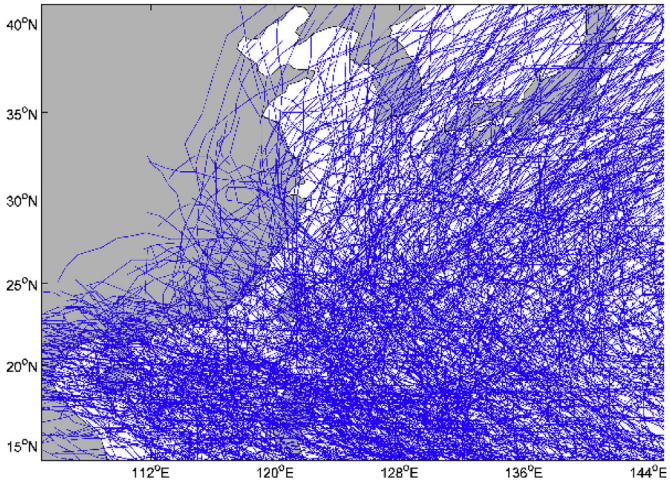

Fig. 13. Typhoon tracks during 1979 and 2013.

location (location A and B) the wave heights calculated by coupled model fluctuate with the change of tidal level, i.e. modulated by tides, and the peak is about 0.3 m larger than the uncoupled model at location A. It is demonstrated the necessity of using the coupled model to estimate the extreme waves in the coastal area. With the increasing of the water depth (location C and D), the wave-current effect during the typhoon period is negligible.

The surge processes simulated by coupled and uncoupled model, i.e. CASE-WC and CASE-TOW, at these four locations are also compared during typhoon Saola, as showed in Fig. 12. It can be seen that the effects of wave-current interaction on the surge are noticeable at near shore area (location A and B) when the typhoon centre approaches the nearshore area, while the effects becomes insignificant at deep water area (location C and D).

From Figs. 11 and 12, it can be seen that the wave-current interaction have noticeable effects on the wave and surge simulations, particularly in the nearshore area during the typhoon-affected period. Therefore, using the coupled modelling framework becomes necessary when estimating the extreme conditions of waves and surges.

5. Long-term wave analysis

Following the model validations, the model was run for long-term simulations of waves and surges from 1979 to 2013. Fig. 13 shows the typhoon tracks over 35 years in the northwest Pacific Ocean. In total, 862 typhoons occurred in this region during this period. To improve the simulation accuracy, the original ECMWF reanalysis data were modified by the parametric typhoon model (Jelesnianski, 1965) using the 35-year best track data. Both the original ECMWF reanalysis data and the modified ECMWF data with the parametric typhoon model (ECMWF-T) were used to drive the model for comparisons (CASE-WC1 & CASE-WC2).

To minimize the boundary effects, the model results from a sub-domain (105°E – 140°E and 15°N - 41°N) were extracted for analysis, over which the spatial and temporal distributions of mean and extreme wave heights and surge levels with 50-year and 100-year return periods

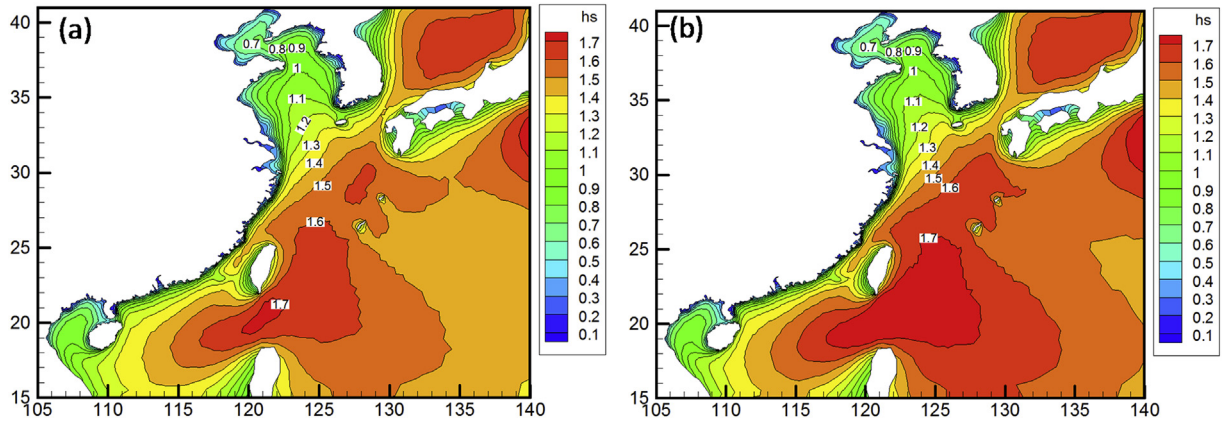

Fig. 14. 35-year mean wave heights generated by (a) ECMWF and (b) ECMWF-T data.

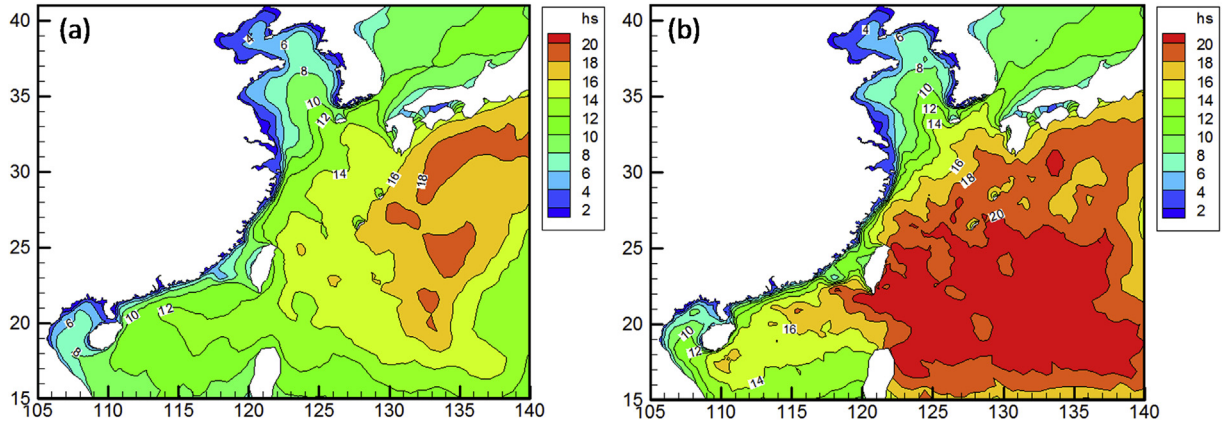

Fig. 15. 100-year return period waves generated by (a) ECMWF and (b) ECMWF-T data.

were calculated. Since the distributions and patterns for both return periods were similar, only the extreme waves and surges with 100-year return period results are presented in this paper.

5.1. Mean wave heights

The mean wave heights were calculated by averaging the computed wave heights over the 35-year simulation period. Fig. 14 shows the 35-year mean wave heights generated by both ECMWF and ECMWF-T wind data in the study area. The results clearly show that the mean wave height generally decreased northwards and landwards. Fig. 14 shows that the mean significant wave height was between 1.3 m and 1.7 m in the north of the South China Sea, 1.2 m–1.5 m in the East China Sea, 0.9 m–1.3 m in the Yellow Sea and less than 1 m in the Bohai Sea. The largest mean wave heights were found southeast of Taiwan Island. By comparing the wave fields generated by the ECMWF and ECMWF-T winds, it can be seen that the distributions of mean wave heights from both winds were generally similar. However, noticeable differences were seen southeast of Taiwan Island, with larger waves generated by the ECMWF-T winds. This is expected and believed to be reasonable because this is the area with a large occurrence of typhoons over the 35-year period as shown in Fig. 13. The results show evidence of the improvement of wind data when the parametric typhoon model was used.

5.2. Extreme wave heights

The annual maximum significant wave heights were extracted from the long-term computed wave heights. The annual maxima were analysed by using the Gumbel distribution method (described in Section 2.2) to calculate the wave heights with a 100-year return period. The extreme wave heights were first estimated by considering the waves in all directions, and the extreme wave heights in 6 main directional sections were then estimated. The directional distributions were particularly important for determining the design waves at different coastal locations. The extreme waves were also calculated in different seasons to explore their seasonal variation.

5.2.1. Distribution of overall extreme waves

The annual maximum wave heights at each grid point were calculated, and the distribution of overall extreme wave heights were then calculated for the entire computational region. Fig. 15 shows the spatial distributions of extreme wave heights generated by ECMWF and ECMWF-T data. It can be seen that the extreme waves decreased from south to north and from sea to coast; the contours appear to be parallel to the coast when approaching it. The extreme waves in the Bohai Sea and the Yellow Sea generated with both ECMWF and ECMWF-T winds were almost the same because typhoon events might not occur so often in these areas (see Fig. 13). It can be seen from Fig. 15 that the 100-year return period wave heights in the Bohai Sea were less than 7 m, whereas those in the Yellow Sea were between 7 m and 11 m. However, in the East China Sea and the northern part of the South China Sea, the extreme wave heights calculated by the ECMWF-T winds were much larger than those from the ECMWF winds, especially in the southeast part of Taiwan Island. This is the area through which many typhoons passed during 1979–2013, as shown in Fig. 13. Because the parametric typhoon model improved the accuracy of wind fields during the typhoon events over the un-modified ECMWF winds, it is reasonable that the extreme waves generated by ECMWF-T wind data were more accurate than those generated by

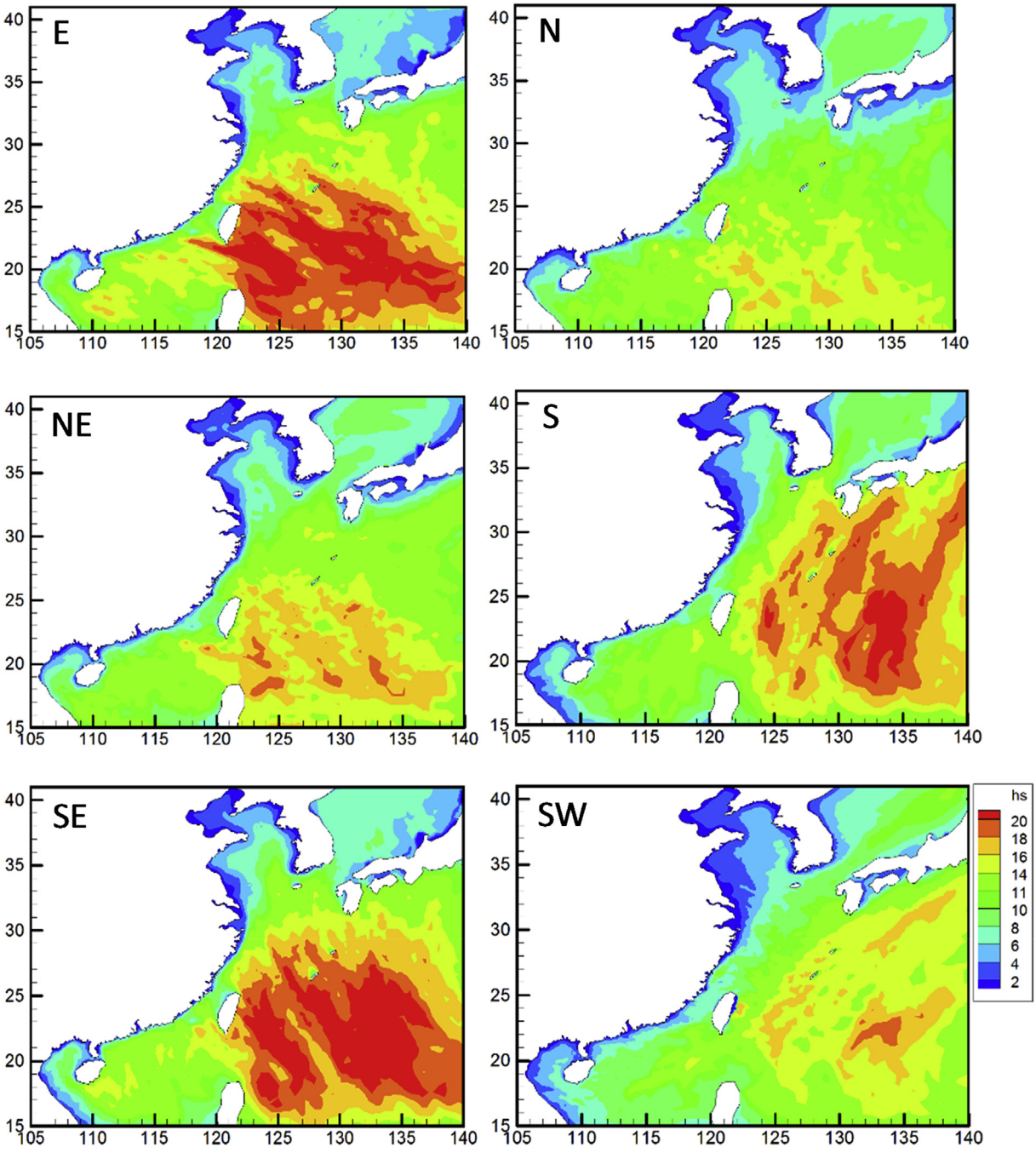

Fig. 16. 100-year return period waves in E/N/NE/S/SE/SW directions generated by ECMWF-T data.

ECMWF wind data.

5.2.2. Directional distribution of extreme waves

Because the directional distribution of extreme waves is of great importance for engineering designs, especially for infrastructure in coastal areas, extreme waves in six landward directional sectors (E, N, NE, S, SE, and SW) were chosen for the study (coming direction for waves). Because the waves generated by ECMWF-T data were more accurate than those generated by ECMWF data, only the extreme waves from ECMWF-T data are presented and discussed here. Fig. 16 shows the spatial distributions of extreme waves in the six directions. Extreme waves in E and SE directions generally had the largest values, followed by those in S direction. Northerly extreme waves were the smallest. The large waves higher than 20 m mainly occurred in the open deep water areas, particularly the area east and south-east of Taiwan Island, similar to those shown in Fig. 15(b). For the extreme waves in E direction, the results showed that larger waves could penetrate much closer to the shore, such as the areas in the eastern coast of China adjacent to Taiwan Island. The extreme waves in SE direction exhibited a similar trend because the large typhoon-induced waves in this study area were mostly from the east or south-east directions, along which a large fetch was available for waves to develop and propagate shoreward in the region.

5.2.3. Distribution of seasonal extreme waves

In the northwest Pacific Ocean, typhoons generally occur in the summer and autumn seasons and cold storm waves occur in the winter and spring seasons. Therefore, typhoon waves may feature strong seasonality, which was also examined in this study. Fig. 17 shows the 100-

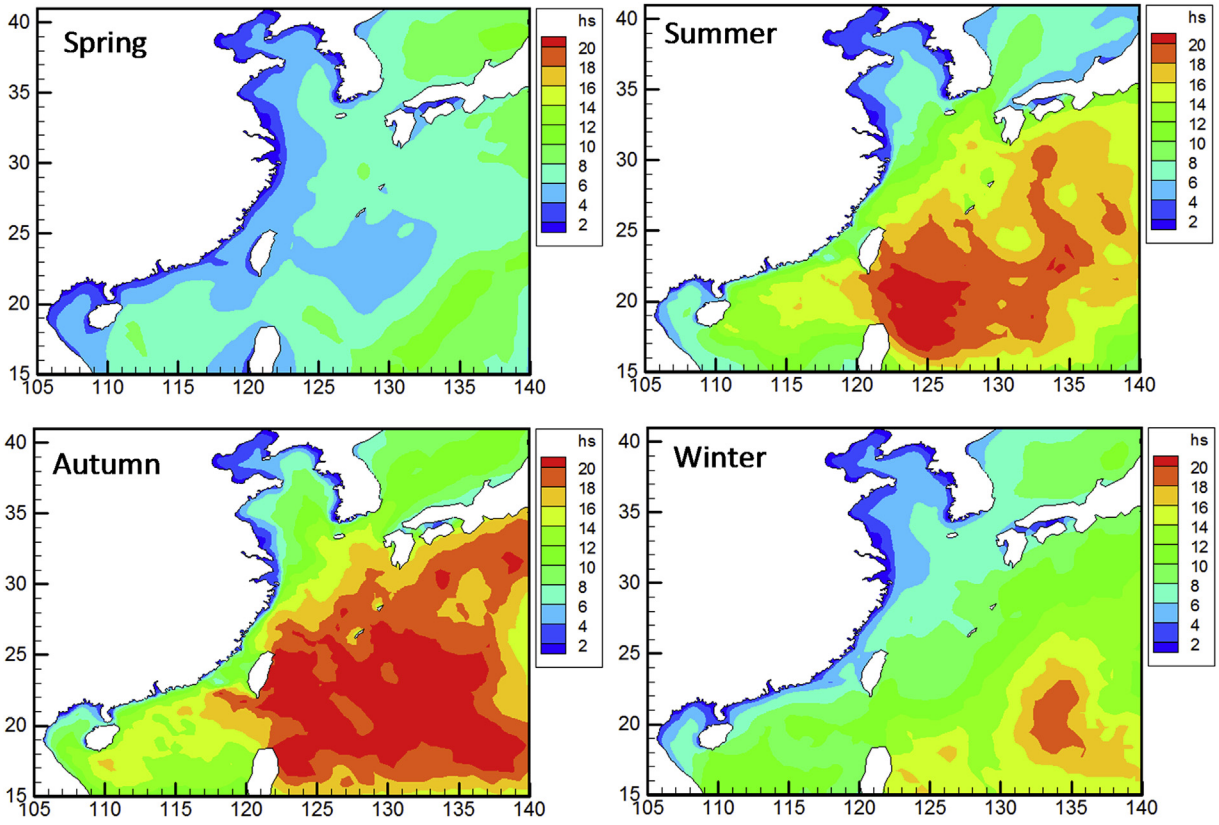

Fig. 17. 100-year return period waves in four seasons generated by ECMWF-T data.

Table 2
Information of long-term wave observation data.

Station	Longitude (°)	Latitude (°)	Water Depth (m)	Data Availability
Laohutan	121.68	38.87	28	1962–2009
Zhimaowan	119.92	40	6	1963–2007
Tianjingang	117.82	38.57	7	1960–1979
Xiaomaidao	120.42	36.05	23.8	1961–1995
Lianyungang	119.43	34.73	9.6	1960–2009
Shengshan	122.82	30.7	40	1960–2009
Dachen	121.9	28.45	15.3	1960–2009
Nanji	121.1	27.42	20	1960–2009
Chongwu	118.93	24.83	11	1962–2009
Dawanshan	113.72	21.93	28.9	1984-1986,1995-2009
Weizhoudao	109.12	21.02	13	1962–2002,2006,2007,2009

year return period wave heights generated by ECMWF-T winds in spring (March, April and May), summer (June, July and August), autumn (September, October and November) and winter (January, February and December) seasons. It can be clearly seen that the extreme wave heights were the smallest in the spring season, whereas larger extreme waves occurred in the summer and autumn seasons resulting from the frequent occurrence of the typhoon events. The largest extreme waves occurred in the east and south-east of Taiwan Island, which is under the path of the majority of the typhoons shown in Fig. 13. It should be noted that the extreme waves in winter were relatively larger than those in summer in the northern area, such as in the Bohai Sea and part of the Yellow Sea, which indicates the existence and impacts of cold winter storms in winter in the north part of the China coasts.

5.2.4. *Extreme waves at nearshore stations*

Extreme waves were gradually reduced shoreward as shown in Fig. 15 and became low in the nearshore areas. However, they remain important for the design of coastal engineering projects, especially at locations of important coastal infrastructure. To examine the accuracy of the estimated extreme waves in the coastal area, the hind-casted extreme wave heights with a 100-year return period were compared with the field measurements taken at several nearshore wave observation stations along the coast of China. The availability of the field data at these stations is summarized in Table 2 and the locations are marked in Fig. 1.

Fig. 18 shows the comparisons of the computed extreme wave heights with the measurements in 6 main directional sectors along the coasts of China. The observational data (denoted as OBS) in Fig. 18 were calculated from the long-term measurements at those stations, as listed in Table 2. Note that the measurement data in some directions were unavailable and are missing in Fig. 18. The results show the general pattern of the extreme wave distributions along the coast of China, clearly showing that the extreme wave heights were relatively small in the northern region and large in the southern region in all directions. For the locations in the south, the extreme waves were the largest in E direction, followed by NE and SE directions, because those areas were exposed to the open seas toward the east so that waves from those directions could directly propagate to the shore over a large fetch without being sheltered. In N direction, the nearshore extreme waves at the mid-eastern coast of China were large and decreased southwards, whereas the nearshore extreme waves in S direction exhibited an opposite trend. The variations can be attributed to the orientation of the shorelines and impacts on wave propagation. It is also interesting that large extreme waves existed in SW direction, although the extreme waves in this direction may often be ignored in engineering designs. The smaller nearshore extreme waves in the northern coasts from Laohutan to Lianyungang (the coastal areas of Bohai Sea and Yellow Sea) are believed to be because of the fewer occurrences of typhoons and shallower water depths in those areas.

Fig. 18 shows that the simulated extreme wave heights agreed well with the observational data at the nearshore locations. The extreme wave heights computed by the ECMWF data were underestimated in most of

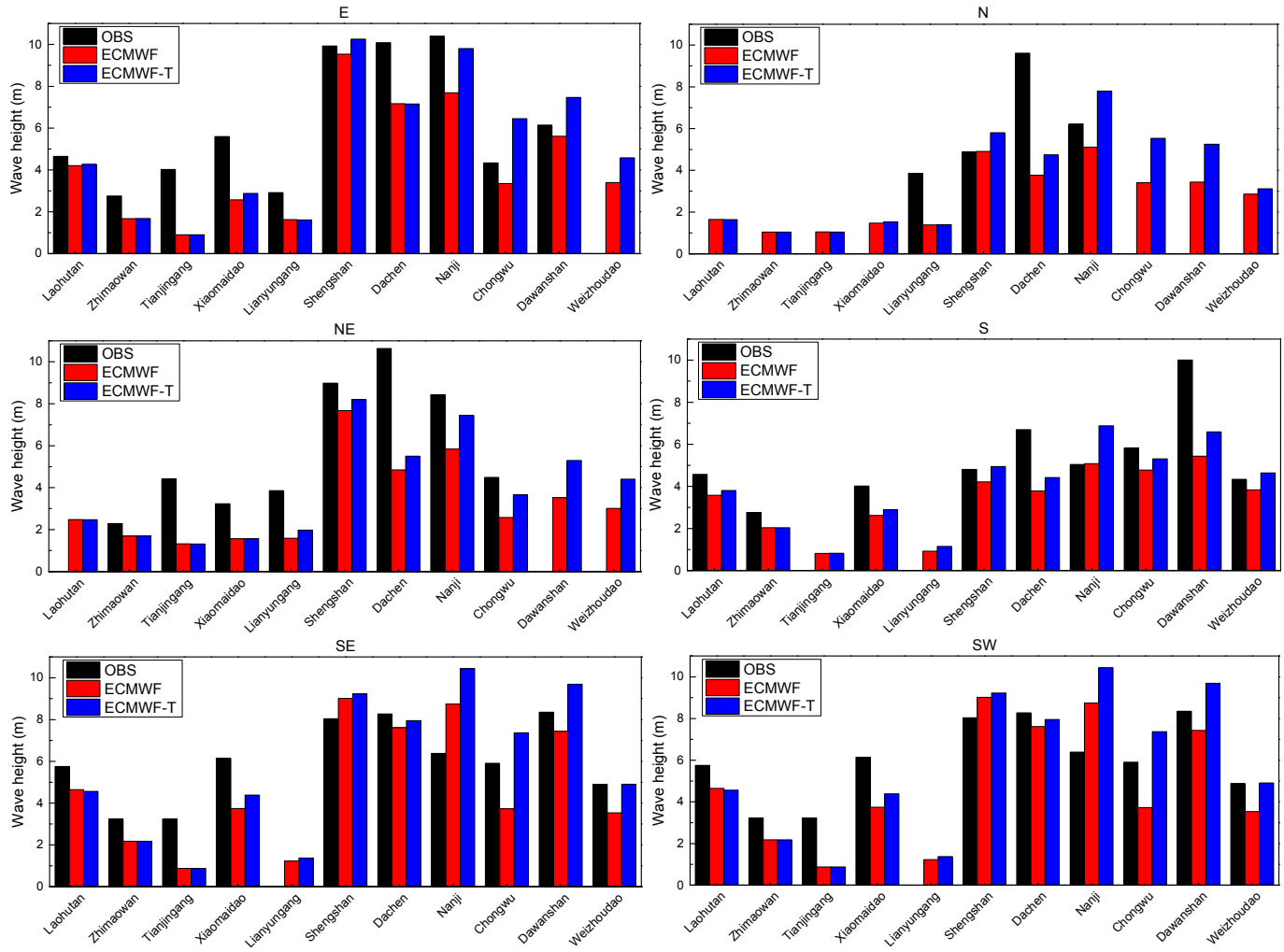

Fig. 18. The comparison of 100-year return period waves between measured and simulated data generated by ECMWF and ECMWF-T wind at 11 nearshore stations.

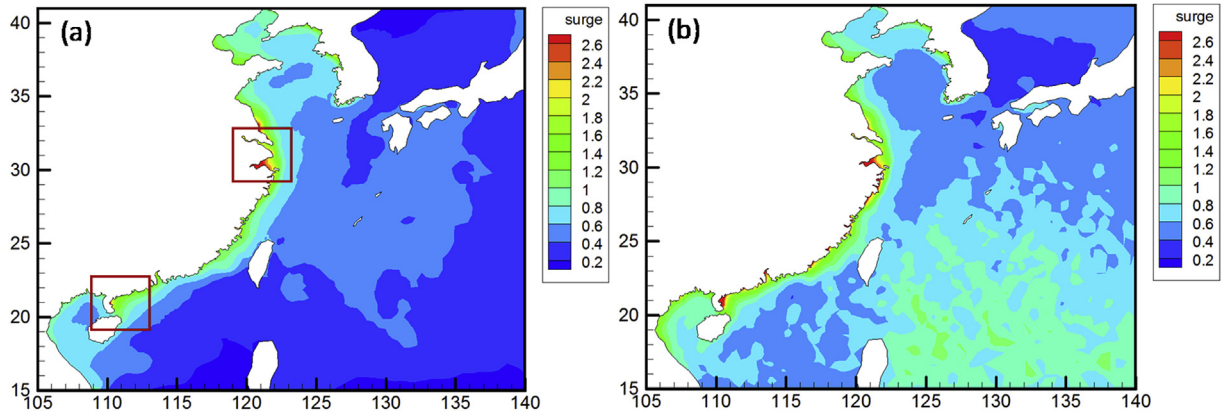

Fig. 19. 100-year return period surge levels generated by (a) ECMWF and (b) ECMWF-T atmospheric data.

the observation stations, whereas the extreme wave heights computed by the ECMWF-T data again clearly indicated an improvement in yielding the extreme values in the nearshore area despite the discrepancies between the measurements and the model results at some stations. For example, the extreme waves from the model were obviously underestimated in Dachen from N to E directions and overestimated in Nanji in SW and SE directions because the resolution of the computational mesh was insufficiently fine to represent the rapid variation of the bathymetry in the nearshore areas; further refinement will be required in future study.

6. Extreme surges

To examine the extreme surge, the water levels computed in the tide-

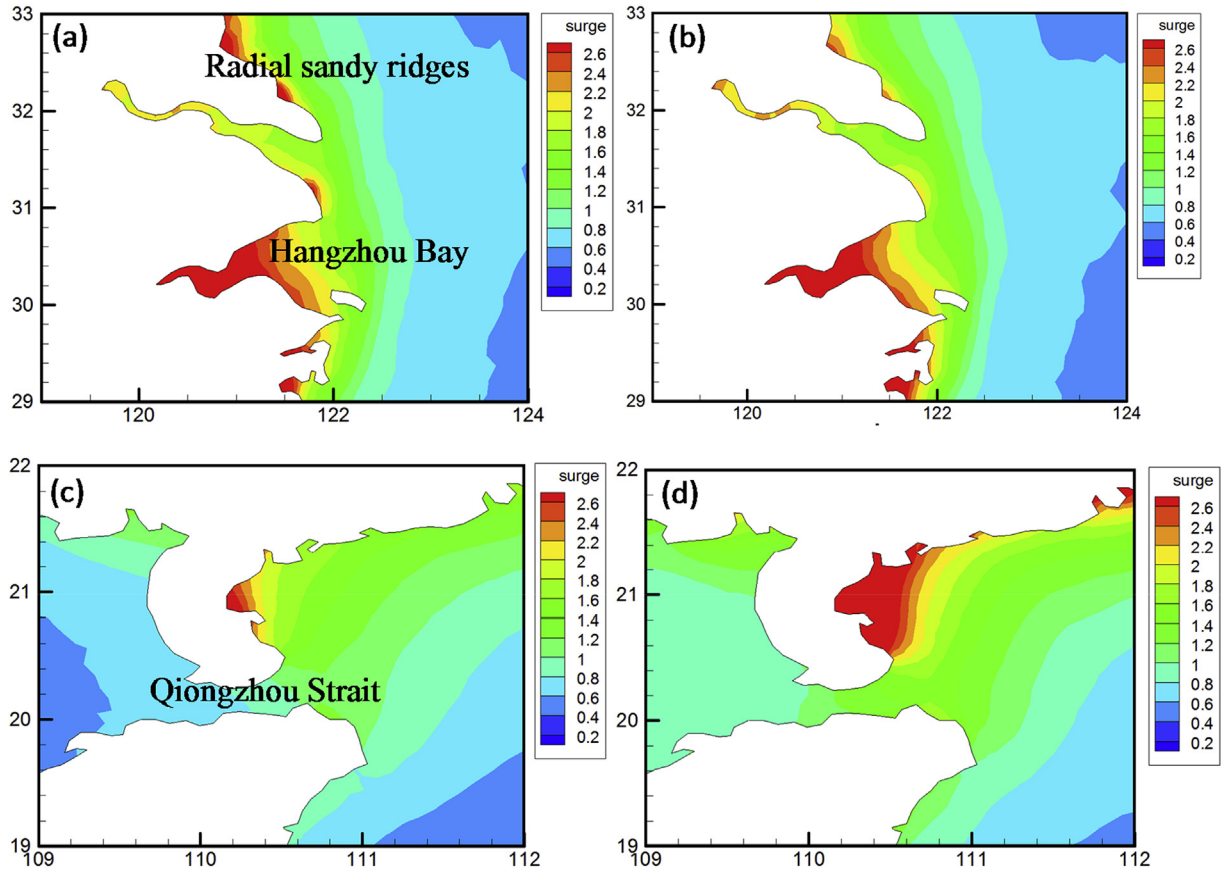

Fig. 20. 100-year return period surge levels generated by ECMWF (left panel) and ECMWF-T (right panel) at Hangzhou Bay (a & b) and Qiongzhou Strait (c & d).

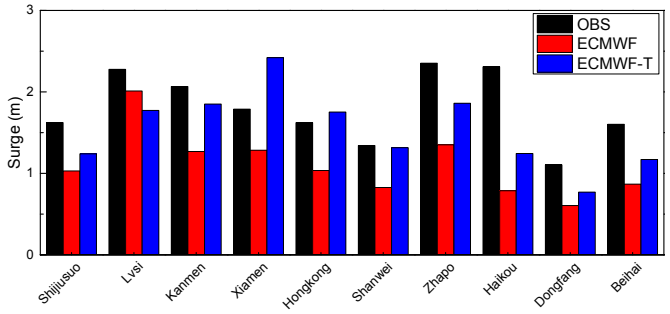

Fig. 21. The comparison of 100-year return period surge levels between measured and simulated data generated by ECMWF and ECMWF-T atmospheric data at 10 nearshore stations.

only case (CASE-TO) were subtracted from those computed in the cases with the combined tide and wave conditions (CASE-WC1 & CASE-WC2). The water level differences (surge levels) calculated were then analysed, and the annual maxima over the 35-year period were used to estimate the extreme surge levels for a 100-year return period at each grid point in the model domain.

6.1. Distribution of extreme surges

Fig. 19 shows the distributions of 100-year return period surges driven by ECMWF and ECMWF-T data over the study region. Comparing the surges generated by the un-modified ECMWF and ECMWF-T data, their distribution patterns are largely similar. The surge levels generated by the ECMWF-T data were slightly larger, as expected. The extreme surges increased towards the coastal waters when water depth decreased. Larger 100-year return period extreme surges were found along the coastline of China from the south of Shandong Peninsula to the Hainan Island (Fig. 1), up to 2 m in general but as large as over 4 m in some areas. The extreme surge levels appear to be closely related to the local bathymetry. The surge level was larger when the water depth was smaller and the extreme surge contours often coincided with the water depth contours. The simulation results suggest that the coastal area in the radial sandy ridge area off the Jiangsu coast, Hangzhou Bay and the north of the Qiongzhou Strait tend to have the relatively large extreme surges. Two particular areas were chosen to illustrate the impacts: the area adjacent to the Hangzhou Bay and the area adjacent to the Qiongzhou Strait, as indicated in Fig. 19(a). Fig. 20 shows the extreme surges in those two areas generated by both ECMWF and ECMWF-T data. The shape of the coastline and the change of the water depth affected the surge level. For example, in Hangzhou Bay, shown in Fig. 20 (a) and (b), the funnel shape of the coastline resulted in the concentration of tidal energy and extremely large surges inside the Bay. Additionally, surges were higher in the area where typhoons frequently occurred, such as in the north of Qiongzhou Strait (see Fig. 20 (c) and (d)). The differences in surges in the area adjacent to Hangzhou Bay were insignificant, whereas there were noticeable differences for surges in the area adjacent to the Qiongzhou Strait. The tide-surge interactions could also make a great contribution to extreme surges in these areas (Feng and Tsimplis, 2014; Zhang and Sheng, 2015), although this is outside the scope of this paper.

6.2. Extreme surges at nearshore stations

To compare the model results with the field measurements in the

nearshore areas specifically, the sea level observations at 10 tide gauges as listed in the UHSLC database (Caldwell et al., 2015) were used. The database contains the measurements for more than 25 years. The Gumbel distribution was applied to the measured surge levels to estimate the extreme values with a 100-year return period. The non-tidal components were extracted from the measured sea levels at these locations using the T_TIDE package introduced in Section 4.3. The comparison of 100-year return period surges between measured data and simulated data driven by ECMWF and ECMWF-T are shown in Fig. 21. In general, the computed surge levels at all stations were close to those from measurements and those generated by the ECMWF-T winds were in better agreement except Lvsi station which may be due to the complicated currents there. Among all 10 stations, the Lvsi, Zhapo and Haikou stations appeared to have the largest values of extreme surge, over 2 m. These three stations are located in the large extreme surge domain discovered in the mapped extreme surge field in Section 6.1. In general, the surges along the coast of China were slightly underestimated, which may have been caused by the rapidly changing water depth and the coarse grid in the nearshore area along the coast of China. Moreover, to some extent the wind discrepancies may have also affected the simulated results. However, the extreme surges simulated by the ECMWF-T data were generally better than those simulated by the original ECMWF data, which further confirms the superiority of modified ECMWF data in the simulation of extreme events in the coastal region of China.

7. Conclusions

This study used the coupled hydrodynamic model FVCOM and the wave model FVCOM-SWAVE to simulate long-term waves and surges for the 35 years from 1979 to 2013 and to estimate the 100-year return period extreme waves and surges in the northwest Pacific Ocean region. The model was forced by tidal conditions provided by the TPXO 7.2 database and atmospheric conditions provided by both the original ECMWF reanalysis data (ECMWF) and the modified ECMWF data (ECMWF-T) with a parametric typhoon model to improve the representation of typhoon events.

The model was validated with field measurements of waves and surges. The results demonstrated that the waves and surges generated by ECMWF-T were in better agreement with the measurements and the adequate implementation of the parametric wave model. The 35-year mean wave heights in the region showed that waves were high in the south and gradually deceased northwards. The largest mean wave heights were located in the area east of Taiwan Island.

The extreme waves and surges with a 100-year return period in the region were estimated from the computed wave heights and surge levels over the 35-year period using the Gumbel Distribution. The results of the spatial distribution showed that the extreme waves in the study area generally decreased northward and shoreward, similar to the mean wave height distributions. The maximum extreme wave heights were also found southeast of Taiwan Island, with values up to 23 m. The distributions of directional and seasonal extreme waves were also examined. The extreme waves in E, SE and NE directions and in summer and autumn seasons appeared to have larger values in most of the deep open water areas. The extreme waves in the SW direction were also found to have large values, which indicated a significant wave propagation parallel to the shoreline in the southern coast of China. The extreme surge levels were found to be significant in the nearshore areas, particularly at the coasts in the Jiangsu radial sandy ridge area, Hangzhou Bay and north of the Qiongzhou Strait. The extreme surges appeared to coincide with the water depth contours, which indicates the effects of local bathymetry on surges.

The results of the 100-year return period wave heights and surges were compared with those calculated from the long-term observational data at a number of locations along the coast of China. The comparisons showed that the waves and surges generated by the modified ECMWF data (ECMWF-T) by the parametric typhoon model agreed better with the measurements and were more accurate than those generated by the original ECMWF reanalysis data.

This study provided detailed insights into the distribution of extreme waves and surges in the northwest Pacific Ocean, especially the coast of China. It has also provided a simple yet effective method to modify the surface forcing, the ECMWF reanalysis data in this case, when simulating waves and water levels with typhoon events. The details of the extreme waves and surges obtained from this study can be easily used for engineering designs at the given locations of interest by longitude and latitude. The simulation results in the coastal area may be further improved with the refinement of the unstructured mesh of the area of interest.

Acknowledgements

The work was partly supported by the National Key R&D Program of China (2017YFC0405401), National Natural Science Foundation of China (51620105005), the Key Research Project of Water Resources Department of Jiangsu province, China (2015006), the 111 Project of the Ministry of Education and the State Administration of Foreign Experts Affairs, China (B12032) and the Fundamental Research Funds for the Central Universities, China (2017B40714, 2017B20214). The first author also would like to thank the China Scholarship Council (201506710061) for the financial support for the 18-month PhD exchange program in Cardiff University.

References

Booij, N., Ris, R.C., Holthuijsen, L.H., 1999. A third-generation wave model for coastal regions: 1. Model description and validation. J. Geophys. Res. 104, 7649–7666.
Beardsley, R.C., Chen, C., Xu, Q., 2013. Coastal flooding in Scituate (MA): a FVCOM study of the 27 December 2010 nor'easter. J. Geophys. Res. 118, 6030–6045.
Caldwell, P.C., Merrfield, M.A., Thompson, P.R., 2015. Sea Level Measured by Tide Gauges from Global Oceans - the Joint Archive for Sea Level Holdings (NCEI Accession 0019568). NOAA National Centers for Environmental Information. Dataset, Version 5.5. .
Castillo, E., 1988. Extreme Value Theory in Engineering. Academic Press Inc., NewYork.
Chen, C., Beardsley, R.C., Cowles, G., 2006a. An unstructured grid, finite-volume coastal ocean model. In: FVCOM User Manual.
Chen, C., Liu, H., Beardsley, R.C., 2003. An unstructured grid, finite-volume, three-dimensional, primitive equations ocean model: application to coastal ocean and estuaries. J. Atmos. Ocean. Technol. 20, 159–186.
Chen, H., Hua, F., Yuan, Y., 2006b. Seasonal characteristics and temporal variations of ocean wave in the Chinese offshore waters and adjacent sea areas. Adv. Mar. Sci. 24, 407–415 (in Chinese).
Chen, Y., Xie, D., Zhang, C., Qian, X., 2013. Estimation of long-term wave statistics in the East China Sea. J. Coast Res. 65, 177–182.
Egbert, G.D., Erofeeva, S.Y., 2002. Efficient inverse modeling of barotropic ocean tides. J. Atmos. Ocean. Technol. 19, 183–204.
Fang, G., Wang, Y., Wei, Z., Choi, B., Wang, X., Wang, J., 2004. Empirical cotidal charts of the Bohai, Yellow, and East China seas from 10 years of TOPEX/poseidon altimetry. J. Geophys. Res.: Oceans 109, C11.
Feng, X., Tsimplis, M.N., 2014. Sea level extremes at the coasts of China. J. Geophys. Res. 119, 1593–1608.
Feng, J., Jiang, W., 2015. Extreme water level analysis at three stations on the coast of the Northwestern Pacific Ocean. Ocean Dynam. 65, 1383–1397.
Guo, Y., Zhang, J., Zhang, L., Shen, Y., 2009. Computational investigation of typhoon-induced storm surge in Hangzhou Bay, China. Estuar. Coast Shelf Sci. 85, 530–536.
Haigh, I.D., Eliot, M., Pattiaratchi, C., 2011. Global influences of the 18.61 year nodal cycle and 8.85 year cycle of lunar perigee on high tidal levels. J. Geophys. Res. 116, C06025.
Hong, H., Li, S., Mara, T., 2013. Performance of the generalized least-squares method for the Gumbel distribution and its application to annual maximum wind speeds. J. Wind Eng. Ind. Aerod. 119, 121–132.
Jelesnianski, P., 1965. A numerical calculation of storm tides induced by a tropical storm impinging on a continental shelf. Mon. Weather Rev. 93, 343.
Jourdain, N.C., Barnier, B., Ferry, N., Vialard, J., Menkes, C.E., Lengaigne, M., Parent, L., 2014. Tropical cyclones in two atmospheric (re) analyses and their response in two oceanic reanalyses. Ocean Model. 73, 108–122.
Kalnay, E., Kanamitsu, M., Kistler, R., Collins, W., Deaven, D., Gandin, L., Zhu, Y., 1996. The NCEP/NCAR 40-year reanalysis project. Bull. Am. Meteorol. Soc. 77, 437–471.
Knaff, J.A., Sampson, C.R., Demaria, M., Marchok, T.P., Gross, J.M., McAdie, C.J., 2007. Statistical tropical cyclone wind radii prediction using climatology and persistence. Wea. Forecast 22, 781–791.
Lee, D.Y., Jun, K.C., 2006. Estimation of design wave height for the waters around the Korean Peninsula. Ocean Sci. J. 41, 245–254.
Li, J., Chen, Y., Pan, S., Pan, Y., Fang, J., Sowa, D.M., 2016a. Estimation of mean and extreme waves in the East China Seas. Appl. Ocean Res. 56, 35–47.

Li, J., Chen, Y., Pan, S., 2016b. Modelling of extreme wave climate in China seas. J. Coast Res. 75 (SI), 522–526.
Li, K., Li, G.S., 2013. Risk assessment on storm surges in the coastal area of Guangdong Province. Nat. Hazard 68, 1129–1139.
Liang, B., Liu, X., Li, H., Wu, Y., Lee, D., 2014. Wave climate hindcasts for the Bohai sea, Yellow sea, and East China sea. J. Coast Res. 32, 172–180.
Liu, J., Sun, L., 2000. Characteristic analysis of wind field and sea wave field in the western part of the N. Pacific Ocean. Mar. Forecasts 17, 54–62 (in Chinese).
Lv, X., Yuan, D., Ma, X., Tao, J., 2014. Wave characteristics analysis in Bohai Sea based on ECMWF wind field. Ocean Eng. 91, 159–171.
Pan, Y., Chen, Y., Li, J., Ding, X., 2016. Improvement of wind field hindcasts for tropical cyclones. Water Sci. Eng. 9, 58–66.
Pawlowicz, R., Beardsley, B., Lentz, S., 2002. Classical tidal harmonic analysis including error estimates in MATLAB using T_TIDE. Comput. Geosci. 28, 929–937.
Qi, J., Chen, C., Beardsley, R.C., Perrie, W., Cowles, G.W., Lai, Z., 2009. An unstructured-grid finite-volume surface wave model (FVCOM-SWAVE): implementation, validations and applications. Ocean Model. 28, 153–166.
Qi, Y., Shi, P., Wang, J., 1997. A preliminary study on characteristics of wind and wave over the central area of Yellow Sea. Mar. Sci. Bull. 16, 1–6 (in Chinese).
Song, D., Wang, X., Zhu, X., Bao, X., 2013. Modeling studies of the far-field effects of tidal flat reclamation on tidal dynamics in the East China Seas. Estuar. Coast Shelf Sci. 133, 147–160.
Tolman, H.L., 1991. A third-generation model for wind waves on slowly varying, unsteady and inhomogeneous depth and currents. J. Phys. Oceanogr. 21, 782–797.
WAMDIG, 1988. The WAM model-A third generation ocean wave prediction model. J. Phys. Oceanogr. 18, 1775–1810.
Wang, Y., Yi, H., 1997. Statistics and spectrum analysis of waves in East China Sea. J. Dalian Fish. Univ. 12, 33–39 (in Chinese).
Wu, L., Chen, C., Guo, P., Shi, M., Qi, J., Ge, J., 2011. A FVCOM-based unstructured grid wave, current, sediment transport model, I. Model description and validation. J. Ocean Univ. China 10, 1–8.
Xu, F., Tao, J., Zhou, Z., Coco, G., Zhang, C., 2016. Mechanisms underlying the regional morphological differences between the northern and southern radial sand ridges along the Jiangsu Coast, China. Mar. Geol. 371, 1–17.
Xu, S., Huang, W., 2011. Estimating extreme water levels with long-term data by GEV distribution at Wusong station near Shanghai city in Yangze Estuary. Ocean Eng. 38, 468–478.
Yao, G., Ma, Z., Ding, B., Wang, J., 1992. Statistical analysis of annual ultimate values of waves in the Yellow Sea and the Bohai Sea. Harb. Eng 4, 31–37 (in Chinese).
Yin, J., Yin, Z.E., Hu, X.M., Xu, S.Y., Wang, J., Li, Z.H., Zhong, H.D., Gan, F.B., 2011. Multiple scenario analyses forecasting the confounding impacts of sea level rise and tides from storm induced coastal flooding in the city of Shanghai, China. Environ. Earth Sci. 63, 407–414.
Yoon, J.J., Shim, J.S., Park, K.S., Lee, J.C., 2014. Numerical experiments of storm winds, surges, and waves on the southern coast of Korea during Typhoon Sanba: the role of revising wind force. Nat. Hazards Earth Syst. Sci. 14, 3279–3295.
Yoon, J.J., Jun, K.C., 2015. Coupled storm surge and wave simulations for the Southern Coast of Korea. Ocean Sci. J. 50, 9–28.
Zhang, H., Sheng, J., 2015. Examination of extreme sea levels due to storm surges and tides over the northwest Pacific Ocean. Cont. Shelf Res. 93, 81–97.
Zhang, W., Hong, H., Shang, S., Chen, D., Chai, F., 2007. A two-way nested coupled tide-surge model for the Taiwan Strait. Cont. Shelf Res. 27, 1548–1567.
Zheng, C., Li, C., 2015. Variation of the wave energy and significant wave height in the China Sea and adjacent waters. Renew. Sustain. Energy Rev. 43, 381–387.